PDE-based Image Interpolators

Youngjoon Cha*, Seongjai Kim** *Regular Members*

ABSTRACT

This article presents a PDE-based interpolation algorithm to effectively reproduce high resolution imagery. Conventional PDE-based interpolation methods can produce sharp edges without checkerboard effects; however, they are not interpolators but approximators and tend to weaken fine structures. In order to overcome the drawback, a texture enhancement method is suggested as a post-process of PDE-based interpolation methods. The new method rectifies the image by simply incorporating the bilinear interpolation of the weakened texture components and therefore makes the resulting algorithm an interpolator. It has been numerically verified that the new algorithm, called the PDE-based image interpolator (PII), restores sharp edges and enhances texture components satisfactorily. PII outperforms the PDE-based skeleton-texture decomposition (STD) approach. Various numerical examples are shown to verify the claim.

Key Words : Interpolator, Approximator, Image Blur, Texture Enhancement, Skeleton-Texture Decomposition (STD)

I. INTRODUCTION

Digital images must often be resampled for various tasks in image processing and computer vision such as image generation, compression, display, and zooming. Image resampling is necessary for every geometric transform of discrete images, except shifts over integer distances or rotations about multiples of 90 degrees; the first step of image resampling is image interpolation. Thus image interpolation methods have occupied a peculiar position in image processing and computer vision[10],[11],[15], [16],[17],[20].

Various interpolation methods have been proposed in the literature. These methods have been traditionally characterized by two kinds: linear and nonlinear ones. For linear methods, diverse interpolation kernels (polynomials) of finite size have been introduced as approximations of the *ideal* interpolation kernel (the sinc function) which is spatially unlimited; see [9], [16], [17], [22], [23]. However, the linear methods perform the interpolation independently of the image content and therefore they may interpolate images crossing edges, which introduces artifacts such as aliasing distortions, image blur, and/or the checkerboard effect. Nonlinear interpolation methods have been suggested in order to reduce the artifacts of linear methods[1],[4],[5],[13],[18]. The major step in the nonlinear methods is to either fi t the edges with some templates or predict edge information for the high resolution image from the low resolution one statistically. These edge-directed methods usually result in sharper interpolated images, but occasionally suffer from severe visual degradation (e.g., bumpy visual impression) in fine texture regions.

Recently, PDE-based methods have been

※ The work of the first author is supported by the National Research Foundation of Korea(NRF) grant funded by the Korea government (MEST) No. 2010-0016427.
The work of the second author is supported in part by NSF grant DMS-0609815.

* Department of Applied Mathematics, Sejong University, Gunja-Dong 98, Seoul 143-747, Korea (yjcha@sejong.ac.kr)
** Department of Mathematics and Statistics, Mississippi State University, Mississippi State, MS 39762-5921, USA (skim@math.msstate.edu)

논문번호 : KICS2010-07-321, 접수일자 : 2010년 7월 23일, 최종논문접수일자 : 2010년 11월 6일

introduced to constrain continuity of edges and reconstruct appropriate sharp edges through iterations[2],[3],[12],[19], beginning from an image interpolated by a conventional interpolation method. These PDE-based methods introduce sharp edges without checkerboard effects; however, they tend to weaken texture components. Note that the resulting PDE-based algorithm, which is a composite of a conventional interpolation and a PDE-based edge-forming, may not be an interpolator but an approximator.

In this article, we will introduce a new texture enhancement method, which can be easily incorporated as a post-process of PDE-based interpolation methods[2],[3]. Here our idea is simple: (1) measure the difference of the edge-formed image (produced by the PDE-based interpolation) and the original image in the low resolution and (2) add its bilinear interpolation to the edge-formed image, in order to make the overall operation an interpolator. In this article, the resulting algorithm will be called the *PDE-based image interpolator* (PII). As we will see, PII has proved superior to the skeleton-texture decomposition (STD) approach[21], a PDE-based interpolation method.

The article is organized as follows. In the next section, after presenting general remarks on interpolation, we briefly review the PDE-based edge-forming method[2],[3] and the skeleton-texture decomposition (STD) approach[21]. Section III introduces the new interpolation method, the PDE-based image interpolator (PII). Its stability and efficiency issues are discussed in detail in the same section. In Section IV, the two texture-enhancing PDE-based interpolation methods (the STD approach and PII) are compared with each other for various images. The proposed approach (PII) has proved superior to the STD approach. Section V concludes our development and experiments.

Ⅱ. PRELIMINARIES

This section begins with general remarks on interpolation. Then, we present a brief review on the PDE-based edge-forming procedure suggested by the authors [2], [3] and the PDE-based skeleton-texture decomposition (STD) approach[21].

2.1 General remarks on interpolation

An interpolation method is called an *interpolator* if the image values are not modified when resampled on the same grid; otherwise it is called an *approximator*. Thus the interpolators can avoid smoothing and preserve high frequencies. It is known that superior kernels are interpolators; even though the converse is not always true.

Interpolation methods applied to image zooming can in general produce higher resolution images if the interpolation is performed appropriately without introducing severe artifacts. A most common approach is to estimate edge information in order not to interpolate crossing edges. Edge-directed methods often produce clearer and sharper edges than linear methods. However, although the interpolation is carried out by an edge-directed method, an edge-forming process is necessary to sharpen edges further. For example, consider a binary image which is separated into two homogeneous regions by a vertical straight line. For this image, the correct edge direction can be easily found, but the information is hard to be incorporated to improve the interpolation quality. It is quite natural to apply one of the linear methods to interpolate the image and therefore the edge in the magnified image will look blurry.

See Figure 1, where a synthetic signal representing the aforementioned binary image is depicted, Figure 1(a), and interpolated by a factor of 3, Figure 1(b). Even though the interpolation is performed appropriately, the interpolated signal appears blurry due to the slow transition on the edge. Such a property can easily make interpolated images (in 2D) look blurry. Thus an edge-forming operation is necessary to apply when interpolation artifacts are to be minimized and an appropriate high resolution has to be achieved. An edge-formed signal is shown in Figure 1(c) along with

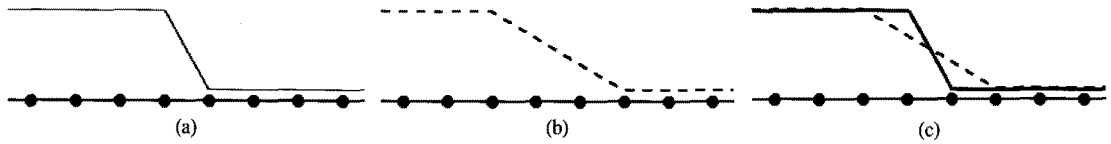

Fig. 1. Interpolation and edge-forming: (a) a synthetic signal, (b) the linearly interpolated signal by a factor of 3, and (c) an edge-formed signal (solid; thick) displayed along with the interpolated signal

the linearly interpolated signal.

The above example shows that an *effective* interpolation algorithm should incorporate an edge-forming operation, because otherwise the edges in the interpolated image may not be sharp enough.

2.2 The PDE-based edge-forming method

In the RGB representation, a color image is a mapping

$$I: \Omega \rightarrow \mathrm{R}_3^+ = \{(r,g,b) : r,g,b \geq 0\},$$

which can be decomposed into brightness and chromaticity:

$$\begin{aligned} \eta(\mathrm{x}) &= \|I(\mathrm{x})\|, \quad \text{(brightness)} \\ \mathrm{u}(x) &= \frac{I(\mathrm{x})}{\|I(\mathrm{x})\|} = \frac{I(\mathrm{x})}{\eta(\mathrm{x})}, \quad \text{(chromaticity)} \end{aligned} \tag{1}$$

where $\|\cdot\|$ is the least-squares (L^2) norm. Thus the brightness η represents the length of the RGB vector and the chromaticity u denotes the normalized color component. It has been verified[6],[7],[14] that in image restoration, the use of the chromaticity-brightness (CB) decomposition

results in better restored images than conventional approaches such as the channel-by-channel model and the HSV system; in particular, the CB decomposition approaches can preserve color components more effectively.

Let

$$\varphi = \tan^{-1}\left(\frac{b}{\sqrt{r^2+g^2}}\right), \quad \xi = \tan^{-1}\left(\frac{g}{r}\right).$$

Associated with the minimization problems

$$\min_{\eta} \int_{\Omega} |\nabla \eta|^p \, dx, \quad \min_{\mathrm{u}} \int_{\Omega} |\nabla \mathrm{u}|^p \, dx, \quad 0 < p < 2 \tag{2}$$

the Euler-Lagrange equations for the brightness and the chromaticity in the angle domain read[14],[25]

$$\begin{aligned} &-\nabla \cdot \left(\frac{\nabla \eta}{|\nabla \eta|^q}\right) = 0, \\ &-\nabla \cdot \left(\frac{\nabla \varphi}{R(\varphi,\xi)^q}\right) = \frac{\sin\varphi \cos\xi}{R(\varphi,\xi)^q} |\nabla \xi|^2, \\ &-\nabla \cdot \left(\frac{\cos^2\varphi \nabla \xi}{R(\varphi,\xi)^q}\right) = 0, \end{aligned} \tag{3}$$

where $q = p-2$ and

$$R(\varphi,\xi) = \sqrt{|\nabla \varphi|^2 + \cos^2\varphi \, |\nabla \xi|^2}.$$

Note that the chromaticity components (φ and ξ) are coupled each other in (3). When $p = q = 1$, the model (2)-(3) becomes a total variation (TV) model. The TV is an indicator for the fluctuation of the image values; the more oscillatory the image is, the bigger the TV becomes. Thus, minimizing the TV is equivalent to smoothing local extrema.

To get an edge-forming model, we first scale the equations in (3) by a factor of $|\nabla \eta|^q$ or $R(\varphi,\xi)^q$, which makes the resulting equations more stable when they are numerically discretized. Then, in order to solve the equations more conveniently, an artificial time t is introduced for the parameterization of the energy descent direction. Finally, we impose a constraint term which enforces the resulting image values to approach the original values at the low resolution image pixels[2]:

$$\begin{aligned}
&\frac{\partial \eta}{\partial t} - |\nabla \eta|^q \nabla \cdot \left(\frac{\nabla \eta}{|\nabla \eta|^q} \right) = \beta_\eta (\eta^0 - \eta), \\
&\frac{\partial \varphi}{\partial t} - R(\phi, \xi)^q \nabla \cdot \left(\frac{1}{R(\varphi, \xi)^q} \nabla \varphi \right) \\
&\qquad = \sin\varphi \cos\xi |\nabla \xi|^2 + \beta_\varphi (\varphi^0 - \varphi), \\
&\frac{\partial \xi}{\partial t} - R(\varphi, \xi)^q \nabla \cdot \left(\frac{\cos^2 \varphi}{R(\varphi, \xi)^q} \nabla \xi \right) = \beta_\xi (\xi^0 - \xi),
\end{aligned} \tag{4}$$

where $(\eta^0, \varphi^0, \xi^0)$ denotes an initialization of (η, φ, ξ) and

$$\beta_\phi = \alpha |\Delta \phi^0|^\delta, \quad \phi = \eta, \varphi, \xi.$$

Here α and δ are positive parameters to be determined. The parameter α is introduced for a global scaling of β_ϕ, while δ must put an emphasis of β_ϕ on fine structures when $\delta > 1$. In practice, we may set $\delta = 3 \sim 5$ and choose α such that the maximum of β_ϕ is about 1000.

In order for the model (4) to be able to form reliable edges, the parameter q must be set larger than 1 (in practice, $q = 1.5 \sim 1.8$) and the diffusion operator in the model must be discretized to show characteristics of anisotropic diffusion. For example, for the one-dimensional version of the brightness model in (4), the diffusion operator can be discretized as

$$\begin{aligned}
\left(\frac{\eta_x}{|\eta_x|^q} \right)_x (x_i) &\approx \frac{1}{d_{i,W}} \eta_{i-1} - \left(\frac{1}{d_{i,W}} + \frac{1}{d_{i,E}} \right) \eta_i \\
&\quad + \frac{1}{d_{i,E}} \eta_{i+1}, \\
|\eta_x|^q (x_i) &\approx 2 \frac{d_{i,W} \cdot d_{i,E}}{d_{i,W} + d_{i,E}},
\end{aligned} \tag{5}$$

where $d_{i,W}$ and $d_{i,E}$ are respectively finite difference approximations of $|\eta_x(x_{i-1/2})|^q$ and $|\eta_x(x_{i+1/2})|^q$ defined by

$$\begin{aligned}
d_{i,W} &= \left[(\eta_i - \eta_{i-1})^2 + \varepsilon^2 \right]^{q/2}, \\
d_{i,E} &= \left[(\eta_{i+1} - \eta_i)^2 + \varepsilon^2 \right]^{q/2} = d_{i+1,W}.
\end{aligned} \tag{6}$$

Here the regularization parameter $\varepsilon > 0$ is introduced to prevent the denominators in (5) from approaching zero and is assumed to be small enough. Note that the right side of the second equation in (5) is the harmonic average of $d_{i,W}$ and $d_{i,E}$.

To solve the model (4) with a great efficiency, we will employ a linearized Crank-Nicolson scheme along with the alternating directional implicit (ADI) procedure[8]. It has been numerically verified that the model (4) incorporating the numerical schemes of anisotropic diffusion (5)-(6) can form reliable edges satisfactorily and efficiently. However, it tends to weaken texture components.

2.3 The PDE-based skeleton-texture decomposition approach

The interpolation method to be presented in this subsection focuses on the interpolation of gray-scale images. For color images, the method can be applied in the channel-by-channel fashion to each of the RGB system, the HSV system, or the CB transformation.

The interpolation method suggested by Saito *et al.*[21] begins with the multiplicative skeleton-texture decomposition (STD)

$$I = U \cdot V + D, \tag{7}$$

where U is the skeleton image, V denotes the texture generator, and D is the construction error. For the decomposition, the authors applied the additive STD method (in the logarithm domain) suggested by Vese and Osher[24]: Minimize the TV-based functional

$$\begin{aligned}
F(u, g) = &\int_\Omega |\nabla u| dx + \mu \int_\Omega |g| dx \\
&+ \lambda \| \ln I - u - \nabla \cdot g \|^2
\end{aligned} \tag{8}$$

where $g = (g_1, g_2)$, uniformly bounded, and μ and λ are positive constants. Let $v = \nabla \cdot g$. The quantities U, V, and D in (7) are defined as

$$U=\exp(u), \quad V=\exp(v), \\ D=I-U\cdot V. \tag{9}$$

Once the decomposition is performed, the three components are interpolated separately. The interpolated image of I, I', is obtained as

$$I'=U'\cdot V'+D', \tag{10}$$

where U' is the interpolation of U carried out by applying the TV-based deblurring-oversampling approach[19], D' denotes a statistically resampled interpolation of D, and V' is the bilinear interpolation of a variation of V, $\widehat{V}$:

$$\widehat{V}=\exp(\kappa(v)) \\ \kappa(v)=v\left[1+(\alpha_M-1)\rho(v)\right], \quad \alpha_M\geq 1, \\ \rho(v)=\begin{cases}(1-v^2/c^2)^2, & \text{if } |v|<c,\\ 0, & \text{if } |v|\geq c.\end{cases} \tag{11}$$

Here α_M determines the upper limit of the strength of the texture enhancement and c is a threshold such that $\kappa(v)=v$ for $|v|\geq c$ and $\kappa(v)\approx\alpha_M v$ for $v\approx 0$. The algorithm (11) has been designed to enhance texture components, but not to introduce over-shooting on texture-packed regions. Thus it enhances texture components more strongly on relatively slow transitions.

It is clear to see that the above STD approach is not an interpolator but an approximator. As a consequence, when V' is set as the interpolation of $V=\exp(v)$, the resultant image I' can be easily blurry. In order to reduce the blurry look, Saito *et al.*[21] introduced the variation of V presented in (11) and therefore they could enhance the texture components by setting c and α_M properly for the given image. However, the overall algorithm is still an approximator and the choice of c and α_M is problematic. The texture enhancement (without the interpolation capability) may introduce artifacts unless the parameters are set appropriately. Furthermore, the approach requires to set many parameters: μ and λ in (8), c and α_M in (11), and a constant and a convolution kernel for the TV-based deblurring-oversampling model[19]. (One may set $\lambda=2$ and $\mu=0.01$ heuristically as in [21], though.)

Ⅲ. THE PDE-BASED IMAGE INTERPOLATOR

For a new texture-enhancing interpolation algorithm, we will begin with the PDE-based edge-forming method presented in Section II-2 and try to make the overall algorithm an interpolator by simply incorporating the bilinear interpolation of the texture components that have been weakened during the edge-forming.

3.1 The algorithm: PII

Let I^* be the solution of the PDE-based edge-forming method presented in Section II-2. Then it can be written as

$$I^*=PI_L^HI, \tag{12}$$

where I is a given image of low resolution, I_L^H denotes a conventional interpolation method from the low resolution to the high resolution (zoom-in), and P is the operator of the PDE-based edge-forming. Let I_H^L be the zoom-out operator, the dual of I_L^H.

We suggest the following algorithm for the texture enhancement:

$$\text{(a) } u=I_H^L I^*, \\ \text{(b) } v=I\ominus u, \\ \text{(c) } I'=I^*\oplus I_L^H v, \tag{13}$$

where I' is the final result, $\oplus$ denotes either addition $(+)$ or multiplication $(\cdot)$, and $\ominus$ is subtraction $(-)$ or division $(\div)$. The functions u and v can be viewed respectively as the skeleton

image and the texture generator of I.

The resulting algorithm incorporating the PDE-based edge-forming operation (12) and the texture enhancement (13) can be written as

$$I' = PI_L^H I \oplus I_L^H(1_L \ominus I_H^L P I_L^H) I, \tag{14}$$

where 1_L is the identity in the low resolution. In this article, the resulting algorithm will be called *the PDE-based image interpolator* (PII). When an integer magnification is considered, the final result I' will have the same values as I at the grids of the low resolution image. Thus PII is an interpolator.

3.2 Stability of PII

It is interesting to consider stability of PII. It has been analyzed[3] that the edge-forming model (4) incorporating the anisotropic diffusion schemes (5)-(6) and a linearized ADI procedure satisfies a *local maximum principle*. By the local maximum principle, we mean the following. When the image is to be zoomed by $(k\times k)$ magnification, on each rectangle of $(k\times k)$ pixels of which four corner pixels correspond to grids of the low resolution image, the interpolated image has its minimum and maximum values on the four corner pixels. That is, there is no local extreme value which is either larger or smaller than the nearest four values of the low resolution image.

Furthermore, the magnified texture generator, $I_L^H v$, satisfies the local maximum principle, because it is a bilinear interpolation of the residual in the low resolution (v). Thus the resulting image I' cannot introduce local extrema inside the rectangles of $(k\times k)$ pixels. Such a maximum principle is important, because otherwise the algorithm may create unnecessary features during the interpolation.

3.3 Implementation of PII

In practice, PII for image zooming can be implemented, without carrying out I_H^L and I_L^H explicitly in (13), as follows:

1) Zoom the given image I to find $\hat{I}$, by employing one of conventional interpolators;
2) Obtain an edge-formed image I^* by applying the edge-forming model (4);
3) Find the difference $\delta = \hat{I} - I^*$ only at the grids of the low resolution image;
4) Interpolate δ to obtain $\hat{\delta}$, by applying the bilinear method for other pixels;
5) Find the final result: $I' = I^* \oplus \hat{\delta}$;

It has been observed that when the magnification factor is set large, the PDE-based edge-forming step (Step II) requires a relatively larger number of ADI iterations. PII converges in $2\sim 3$ iterations for (2×2) magnification and $3\sim 5$ iterations for (3×3) magnification, while it takes $15\sim 20$ iterations for (6×6) magnification. Thus, PII can be carried out by multiple applications of smaller magnification factors in order to speed up the computation. For example, when the image is to be zoomed by a factor of (6×6), the zooming can be performed by (3×3) magnification followed by (2×2) magnification. Since the earlier interpolation, (3×3) magnification, is carried out on a smaller domain, the total computational cost is not much larger than that of the later interpolation, (2×2) magnification. PII is an optimal algorithm; it is an interpolator, converges fast, and can yield sharp edges, as we will see in the next section.

Ⅳ. NUMERICAL EXPERIMENTS

This section presents image zooming examples which show effectiveness of the PDE-based image interpolator (PII) and its superiority to the skeleton-texture decomposition (STD) approach, for both gray-scale and color images. For PII, we set $q=1.5$ and $\varepsilon=0.05$. The texture generator is incorporated additively, i.e., $\oplus$ and $\ominus$ denote respectively addition and subtraction in (13). (The multiplicative texture generation shows no apparent difference from the additive one for most cases; the additive one is occasionally better

slightly.) For the STD approach, the threshold c in (11) is set to be the arithmetic average of $|v|$. For both algorithms, we have employed the same linearized Crank-Nicolson ADI procedure, with the timestep size $\Delta t = 1$, and the strategy of recursive applications of smaller magnification factors in order to speed up the computation.

In the following figure, we will first analyze effects of the parameter α_M (11) introduced for the STD approach to enhance the texture components on relatively slow transitions, and then compare the STD approach with our new algorithm, PII.

Figure 2 shows numerical results from the two algorithms: the STD approach[21] and the proposed method, PII. In order to see how the parameter α_M affects the texture enhancement capability of the STD approach, Figures 2(a)~2(c) depict the interpolated images processed by the STD approach with $\alpha_M = 1$, $\alpha_M = 1.6$, and $\alpha_M = 2.0$, respectively. As one can see from these three figures, the STD approach tends to yield images of higher contrast as α_M increases. However, the overall image quality is not improved satisfactorily. The image in Figure 2(c) shows stronger texture components than those in Figures 2(a) and 2(b), but it involves also apparent artifacts due to an over-shooting on slow transitions; see e.g. a vicinity located between the nose and the left eye. Note that the texture enhancement scheme in (11) is designed to enhance texture components, focusing on slow transitions, and that the resulting algorithm of the STD approach is an approximator. On the other hand, the new method has reproduced clear edges and texture components in high resolution satisfactorily over the whole image domain. In particular, around eyes and the nose, PII assigns much clearer features than the STD approach.

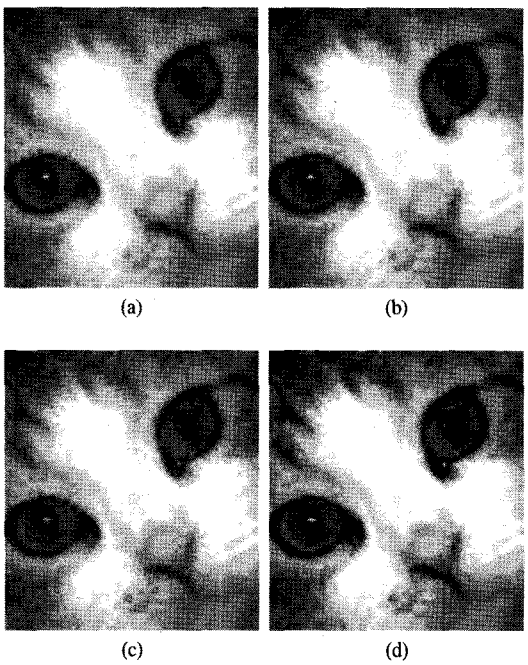

(a) (b)

(c) (d)

Fig. 2. Cat Face (color): (6×6)-magnified images by the STD approach with (a) $\alpha_M = 1$, (b) $\alpha_M = 1.6$, (c) $\alpha_M = 2.0$, and (d) by PII

We have found that the parameters c and α_M introduced in (11) are problematic and for many cases, their choices make little improvement in image quality. We believe that the operation in (11), which simply magnifies the oscillatory patterns, is not a desirable solution for the texture enhancement. In the following, the STD approach is performed with $\alpha_M = 1$.

In Figure 3, we present zoomed images of (Tiffany''s) Eye processed by the two algorithms. As one can see from the figure, the new algorithm has produced clearer texture components and better contrasts. See particularly around the eyebrow and the eyelash. This example shows again that the new texture-enhancing interpolation algorithm (an interpolator) can bring out zoomed

(a) (b)

Fig. 3. Eye (color): (4×4)-magnified images by (a) the STD approach with $\alpha_M = 1$ and (b) PII

(a) (b)

Fig. 4. Lena (gray-scale): (8×8)-magnified images by (a) the STD approach with $\alpha_M=1$ and (b) PII

images more satisfactorily than the STD approach (an approximator).

It should be noticed that the STD approach is more expensive than PII, due to the additional operation of skeleton-texture decomposition which solves the associated Euler-Lagrange equations of (8). See [24] for details.

Figure 4 depicts zoomed images of Lena in gray-scale magnified by a factor of (8×8), by employing three recursive applications of (2×2) magnification. Again, the suggested method is superior to the STD approach for this example. See the left upper part of the image and eyes; the new method has demonstrated texture components of higher contrast. With the new interpolation algorithm, the zoomed image has successfully gained a desirable high resolution on both edges and texture components.

The following examples will show effectiveness of PII in the reproduction of both sharp edges and clear texture components.

Figure 5 depicts zoomed images of Zebra Neck, magnified by a factor of (4×4) by (a) the bilinear interpolation and (b) PII. PII has utilized the image in Figure 5(a) as the basic interpolation and employed two recursive applications of (2×2) magnification. As one can see from the figure, PII has successfully introduced a desirable high resolution on texture regions and reduced the checkerboard effects quite effectively. The stripes in Figure 5(b) particularly look better than those in Figure 5(a).

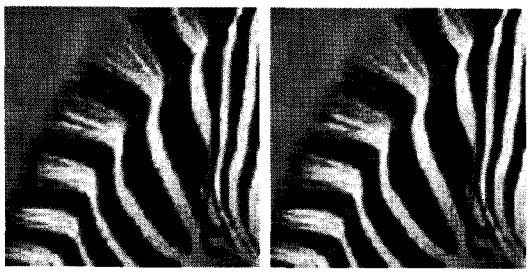

(a) (b)

Fig. 5. Zebra Neck (gray-scale): (4×4)-magnified images by (a) the bilinear interpolation and (b) PII

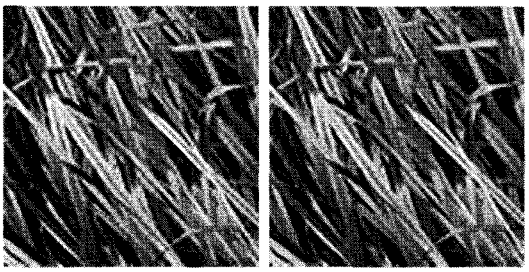

(a) (b)

Fig. 6. Grass (color): (4×4)-magnified images by (a) the bicubic interpolation and (b) PII

Figure 6 depicts zoomed images of Grass, magnified by a factor of (4×4) by (a) the bicubic interpolation and (b) PII. As in the previous example, PII has utilized the image in Figure 6(a) as the basic interpolation. Again, it has successfully reduced the checkerboard effects, while reproducing clear texture components, to get a better image from the basic image interpolated by the bicubic method.

V. CONCLUSIONS

Conventional PDE-based interpolation methods can produce sharp edges without the checkerboard effect; however, they tend to weaken texture components. In order to overcome the drawback, this article has introduced a simple texture enhancement technique to be employed as a post-process of conventional PDE-based methods. The texture enhancement has been carried out for the resulting image just to preserve the image values at the grids of the low resolution image. Thus the resulting algorithm, called the *PDE-based image interpolator* (PII), is an interpolator. It has been verified that PII is more

effective than the PDE-based skeleton-texture decomposition (STD) approach[21] in both efficiency and the reproduction quality of fine structures. From various numerical experiments, we have reached the conclusion that a PDE-based edge-forming method can be effective in the interpolation and satisfactory in the texture enhancement, when it is simply modified to become an interpolator.

REFERENCES

[1] W. Carey, D. Chuang, and S. Hemami, "Regularity-preserving image interpolation," *IEEE Trans. Image Process.*, Vol.8, No.9, pp.1293-1297, 1999.

[2] Y. Cha and S. Kim, "Edge-forming methods for color image zooming," *IEEE Trans. Image Process.*, Vol.15, No.8, pp.2315-2323, 2006.

[3] Y. Cha and S. Kim,, "Edge-forming methods for image zooming," *J. Math. Imaging and Vis.*, Vol.25, No.3, pp.353-364, 2006.

[4] Y. Cha and S. Kim,, "Error-amended sharp edge (EASE) schemes for image interpolation," in *Proceedings of the 13th IEEE International Conference on Image Processing*, 2006, pp.701-704.

[5] Y. Cha and S. Kim,, "The error-amended sharp edge (EASE) scheme for image zooming," *IEEE Trans. Image Process.*, Vol.16, No.6, pp.1496-1505, 2007.

[6] T. F. Chan, S. H. Kang, and J. Shen, "Total Variation Denoising and Enhancement of Color Images Based on the CB and HSV Color Models," *Journal of Visual Communication and Image Representation*, Vol.12, pp.422-435, 2001.

[7] T. F. Chan and J. Shen, "Variational restoration of non-flat image features: Models and algorithms," *SIAM Journal of Applied Mathematics*, Vol.61, No.4, pp.1338-1361, 2000.

[8] J. Douglas, Jr. and S. Kim, "Improved accuracy for locally one dimensional methods for parabolic equations," *Mathematical Models and Methods in Applied Sciences*, Vol.11, pp.1563-1579, 2001.

[9] R. Gonzalez and R. Woods, Digital Image Processing, 2nd Ed. Upper Saddle River, New Jersey: *Prentice- Hall, Inc.*, 2002.

[10] G. Grevera and J. Udupa, "An objective comparision of 3-D image interpolation methods," *IEEE Trans. Medical Imaging*, Vol.17, No.4, pp.642-652, 1998.

[11] G. Grevera and J. Udupa, "A tack- specific evaluation of three dimens- ioal image interpolationtechniques," *IEEE Trans. Medical Imaging*, Vol.18, No.2, pp.137-143, 1999.

[12] F. Guichard and F. Malgouyres, "Total variation based interpolation," in *Proceedings of the Ninth Euro- pean Signal Processing Conference*, Patran, Greece, 1998, pp.1741-1744.

[13] K. Jensen and D. Anastassiou, "Subpixel edge localization and the interpolation of still images," *IEEE Trans. Image Process.*, Vol 4, No.3, pp.285-295, 1995.

[14] S. Kim, "PDE-based image restoration: A hybrid model and color image denoising," *IEEE Trans. Image Processing*, Vol.15, No.5, pp.1163-1170, 2006.

[15] C. Lee, M. Eden, and M. Unser, High-quality image resizing using oblique projection operators," *IEEE Trans. Image Process.*, Vol.7, No.5, pp.679-692, 1998.

[16] T. Lehmann, C. G¨onner, and K. Spitzer, "Survey: Interpolation methods in medical image processing," *IEEE Trans. Medical Imaging*, Vol.18, No.11, pp.1049-1075, 1999.

[17] T. Lehmann, C. G¨onner, and K.Spitzer, "Addendum: B-spline interpol- ation in medical image processing," *IEEE Trans. Medical Imaging*, Vol.20, No.7, pp.660-665, 2001.

[18] X. Li and M. Orchard, "New edge-directed interpolation," *IEEE Trans. Image Process.*, Vol.10, No.10, pp.1521-1527, 2001.

[19] F. Malgouyres and F. Guichard, Edge direction preserving image zooming: A mathematical and numerical analysis," *SIAM J. Numer. Anal.*, Vol.39, pp.1-37, 2001.

[20] G. Penney, J. Schnabel, D. Rueckert, M.

Viergever, and W. Niessen, "Registration-based interpolation," *IEEE Trans. Medical Imaging,* Vol.23, No.7, pp.922-926, 2004.

[21] T. Saito, Y. Ishii, Y. Nakagawa, and T. Komatsu, "Adaptable image interpolation with skeleton-texture separation," in *Proceedings of the 13th IEEE International Conference on Image Processing*, 2006, pp.681-684.

[22] P. Th´evenaz, T. Blu, and M. Unser, "Interpolation revisited," *IEEE Trans.Medical Imaging*, Vol.19, No.7, pp.739-758, 2000.

[23] M. Unser, A. Aldroubi, and M. Eden "Enlargement and reduction of digital images with minimum loss of informa-tion," *IEEE Trans. Image Process.*, Vol.4, No.3, pp.247 -257, Mar., 1995.

[24] L. Vese and S. Osher, "Modeling textures with total variation minimi-zation and oscillating patterns in image processing," *J. Sci. Comput.* Vol.19, pp.553--572, 2003.

[25] L. A. Vese and S. J. Osher, "Numeri-cal methods for p-harmonic flows and applications to image processing," *SIAM J. Numer. Anal.*, Vol.40, No.6, 2002.

Youngjoon Cha Regular Member

Professor, Department of Applied Mathematics, Sejong University

1988, B.S., Department of Mathematics, Seoul National University

1990, M.S., Department of Mathematics, Seoul National University

1997, Ph.D., Department of Mathematics, Purdue University

<Research Interests> Image Processing & Computer Vision, Epidemiology, Wave Simulation

Seongjai Kim Regular Member

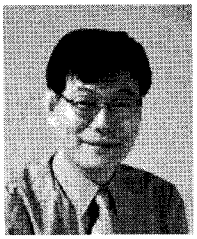

Associate Professor, Department of Mathematics and Statistics, Mississippi State University

1988, B.S., Department of Mathematics, Seoul National University.

1990, M.S., Department of Mathematics, Seoul National University.

1995, Ph.D., Department of Mathematics, Purdue University.

<Research Interests> Image Processing & Computer Vision, Computational seismology, Wave Simulation